Liquid Crystals
Publication details, including instructions for authors and subscription information:
http://www.informaworld.com/smpp/title~content=t713926090

The effect of the position of lateral fluoro-substituents on the stability of the $S^*_{C\alpha}$ and S^*_{CA} phases

V. Faye[a]; J. C. Rouillon[a]; C. Destrade[a]; H. T. Nguyen[a]
[a] Centre de Recherche Paul Pascal, Pessac Cedex, France

To cite this Article Faye, V. , Rouillon, J. C. , Destrade, C. and Nguyen, H. T.(1995) 'The effect of the position of lateral fluoro-substituents on the stability of the $S^*_{C\alpha}$ and S^*_{CA} phases', Liquid Crystals, 19: 1, 47 — 56
To link to this Article: DOI: 10.1080/02678299508036719
URL: http://dx.doi.org/10.1080/02678299508036719

LIQUID CRYSTALS, 1995, VOL. 19, NO. 1, 47–56

The effect of the position of lateral fluoro-substituents on the stability of the $S^*_{C_\alpha}$ and $S^*_{C_A}$ phases

by V. FAYE, J. C. ROUILLON, C. DESTRADE and H. T. NGUYEN*
Centre de Recherche Paul Pascal, Av. A. Schweitzer,
F 33600 Pessac Cedex, France

(*Received 24 October 1994; accepted 28 December 1994*)

Four new chiral series with benzoate cores have been synthesized and characterized. The mesomorphic properties have been analysed by optical microscopy on the pure enantiomeric and the racemic compounds and on mixtures, by D.S.C. and by electro-optic measurements. Three of the series (hydrogenous, monofluoro-substituted *ortho* to the alkoxy chain, and difluoro-substituted) display a very rich polymorphism including S_A, $S^*_{C_\alpha}$, S^*_C, $S^*_{C_{FI}}$ and $S^*_{C_A}$ phases, whereas the series monofluoro-substituted in the *meta*-position does not exhibit $S^*_{C_{FI}}$ and $S^*_{C_A}$ phases any more except for the dodecyloxy derivative, but gives a large enantiotropic $S^*_{C_\alpha}$ phase. A comparison of these four series leads to a discussion about the effect of the transverse dipole moment on the existence of the $S^*_{C_A}$ phase.

1. Introduction

Since the discovery of antiferroelectricity in liquid crystals by Chandani *et al.* [1], in 1989, $S^*_{C_A}$ phases have been paid much attention, especially for their display applications. A large number of compounds exhibiting these phases have been synthesized; a recent review by Fukuda *et al.* [2], mentioned more than 300 compounds.

Up to now, the structure of $S^*_{C_{FI}}$ and $S^*_{C_\alpha}$ phases is not clear, and their study is always complicated by their short temperature ranges. Therefore, the search for new materials and an understanding of the chemical parameters responsible for the appearance of $S^*_{C_A}$, $S^*_{C_{FI}}$ and $S^*_{C_\alpha}$ phases seems to be necessary.

In this study, we explore the influence of the benzoate ester core and fluorine substitution of the first phenyl ring of the 4-alkoxybenzoate moiety on the stabilization of these tilted smectic phases in the series compounds:

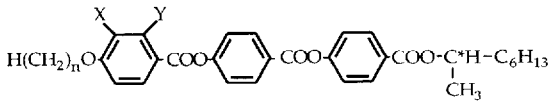

$X = Y = H$	*n*HHBBM7 (*n*HH series)
$X = F, Y = H$	*n*FHBBM7 (*n*FH series)
$X = H, Y = F$	*n*HFBBM7 (*n*HF series)
$X = Y = F$	*n*FFBBM7 (*n*FF series)

* Author for correspondence.

2. Materials

The synthetic route is briefly summarized below:

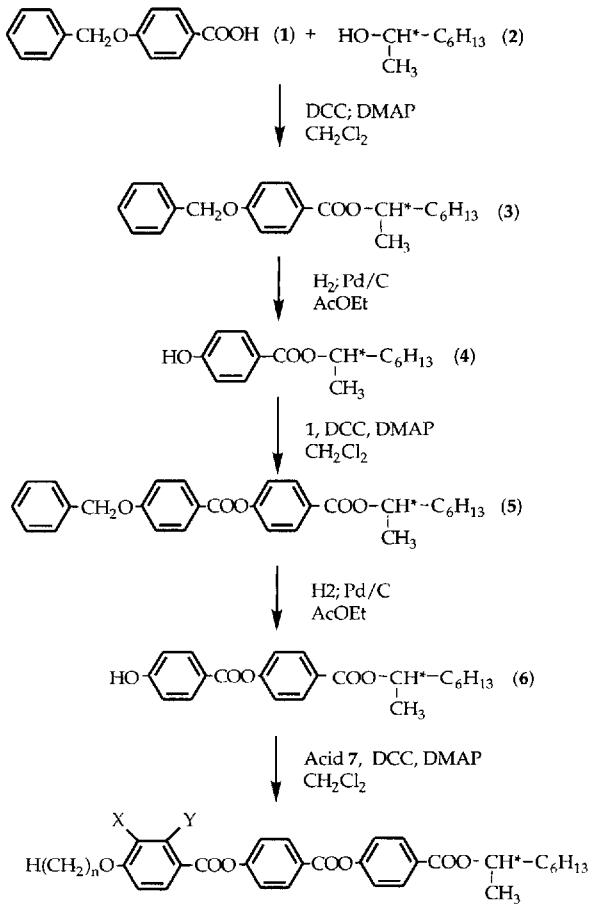

The acid **1** is obtained by an etherification reaction

0267–8292/95 $10·00

Table 1. Transition temperatures (°C) and enthalpies (kJ mol^{-1}) (in italics) for the *n*HH series (positive enthalpy values are given for heating scans; negative ones are for cooling scans).

n	Cr		S^*_{CA}		S^*_{CFI1}		S^*_{CFI2}		S^*_C		S^*_{Cz}		S_A		I
7	•	82·8 *30·8*	—		—		—		•	(69·8)	•	(72·6) *− 0·023*†	•	141·9 *− 5·73*	•
8	•	89·05 *34·7*	•	(58·4) *− 0·003*	•	(74·5) ?	•	(87·8) *− 0·003*	•	90·8	•	94·4 *− 0·47*†	•	139·7 *− 5·51*	•
9	•	95·8 *38·6*	•	(90·1) *− 0·009*	•	(92·2) *− 0·002*	•	97·2 *− 0·009*	•	106·6	•	109·2 *− 0·14*†	•	136·0 *− 5·36*	•
10	•	90·3 *34·5*	•	99·2 *− 0·006*	•	100·6 *− 0·002*	•	102·7 *− 0·016*	•	114·3	•	115·3 *− 0·252*†	•	135·5 *− 5·23*	•
11	•	82·5 *34·4*	•	86·2	•	90·8	•	92·7 *− 0·010*	•	117·4 *− 0·160*	—		•	131·4 *− 5·08*	•
12	•	72·0 *34·9*	•	85·6	•	87·5	•	92·3	•	119·2 *− 0·290*	—		•	131·5 *− 5·30*	•

† Sum of transition enthalpies.
Parentheses denote a monotropic transition.

between benzyl bromide and ethyl 4-hydroxybenzoate, following by saponification and by acid hydroloysis. Its esterification with (*R*)-octan-2-ol in the presence of 1,3-dicyclohexylcarbodiimide (DCC) and 4-*N*,*N*-dimethylaminopyridine (DMAP) as catalyst. The deprotection of the phenolic group is achieved through a palladium catalysed hydrogenolysis reaction. The phenol **4** is added to the acid **1** and the same procedure is repeated in order to lengthen the molecule by one phenyl ring.

The final compounds are obtained by a classical esterification reaction between the phenol **6** and various hydrogenous or fluorinated 4-alkoxybenzoic acids **7**. The mono-and di-fluoroalkoxybenzoic acids were prepared following well-known methods described previously [3, 4].

Compounds **3** and **5** and the final compounds were purified by column chromatography (Merck 60 silica gel) with toluene as eluent for the former and dichloromethane for the latter. All of the products were finally recrystallized from absolute ethanol. The purities of all intermediates and final compounds were checked by thin layer chromatography (using Merck plastic sheets, silica gel 60) and by normal-phase HPLC for the latter. A Waters 600E system controller, in conjunction with a Waters 484 UV–VIS detector, was used. The chromatography was carried out over silica gel (Waters Microporasil, 10 µm particle size, 3·9 mm × 300 mm) using a mixture of heptane and ethyl acetate (9 : 1) as eluent. Detection of the eluting products was achieved using a Waters 484 UV–VIS detector (λ = 254 nm). Each of the final products was found to have a chemical purity exceeding 99·5 per cent.

The chemical structures of all products were checked by nuclear magnetic resonance spectroscopy (Bruker ARX 300) and by Fourier Transform Infrared spectroscopy (Nicolet MX-1).

3. Mesomorphic properties

3.1. *Analysis*

All the compounds are mesomorphic. Microscopic observations were carried out with a Zeiss Ortholux polarizing microscope equipped with a Mettler FP5 hotstage, and calorimetric studies with a Perkin–Elmer DSC7. Slight differences between those two methods of measurement are partly due to instrumental factors and difficulties in distinguishing some transitions.

Heating rates were 5°C min^{-1} for the melting process and cooling rates were 3°C min^{-1} for other transitions. When transition enthalpies were too weak to be detected, the temperatures given are those observed optically.

3.2. *Hydrogenous compounds*

3.2.1. *Optical textures*

Transition temperatures are given in table 1 and an example of a DSC diagram is shown in figure 1.

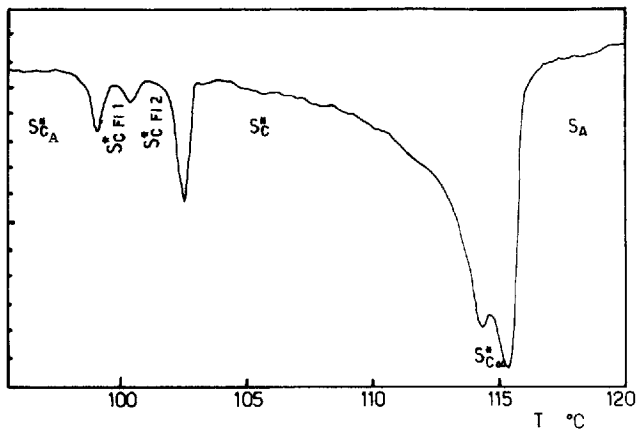

Figure 1. DSC diagram of 10HH at a cooling rate of 3°C min^{-1}.

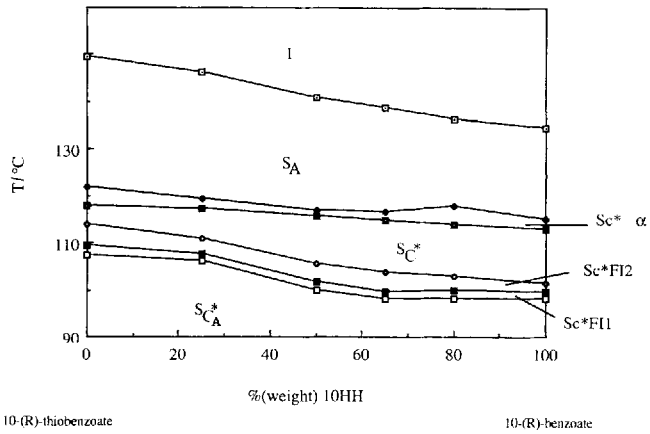

Figure 2. Isobaric diagram showing the isomorphy of the phases of 10HH and its thiobenzoate homologue.

On cooling from the isotropic liquid for the 10HH compound, the homeotropic and focal-conic textures of a S_A phase are found. The $S^*_{C_\gamma}$ phase is hardly detectable by microscopic observation because its texture is similar to that of the S_A phase, may be due to the low tilt angle. Its existence is shown by DSC and with a planar alignment. Then the ferroelectric phase appears with a striated fan shaped or coloured pseudo-homeotropic texture. Further cooling produces a transition to the ferrielectric phases, which show a typical texture in the homeotropic part of the cell; the texture constantly moves, due to the helical pitch changes. We call the phases S^*_{CFI1} and S^*_{CFI2} because, although they have the same texture and the same electro-optic behaviour (see § 4) we can detect a transition between the two phases by DSC. The transition enthalpy is very low (about 0·002 kJ mol^{-1}). As the temperature is lowered, the antiferroelectric phase appears. It looks just like a ferroelectric phase. The photomicrographs of these smectic phases are similar to those given in previous articles [5, 6].

A planar alignment allows one to distinguish ferro- from antiferro-electric phases, but not to detect ferrielectric phases. It also reveals an intermediate phase between S_A and S^*_C (when $n \leqslant 10$): the $S^*_{C_\gamma}$ phase. There, the homogeneous coloured aspect of the S_A phase becomes striated with thin, dark, clear bands parallel to the rubbing direction. In the S^*_C phase, little perpendicular lines appear. The transition to the $S^*_{C_A}$ phase is detected by a radical change of the texture. The new texture replaces the other by large stripes growing perpendicular to the rubbing direction.

3.2.2. *Miscibility studies*

In order to confirm the presence of the ferri- and antiferro-electric phases of these compounds, a miscibility test was performed between 10HH(R) and the corresponding thiobenzoate derivative which was earlier found to exhibit the same mesophases [5], which were themselves miscible with those of MHPOBC. The transition temperatures of this compound are: Cr 109·7 $S^*_{C_A}$ 112 S^*_{CFI1} 114 S^*_{CFI2} 119·2 S^*_C 120·3 $S^*_{C_\gamma}$ 123·6 S_A 132·6 I.

An isobaric binary diagram (see figure 2) was obtained. The mixtures were made by weighing each component and mixing them in their isotropic states.

The phase diagram shows continuous miscibility across the whole composition range for all the phases. Their nature is therefore confirmed.

3.2.3. *Phase behaviour*

Figure 3 shows the phase behaviour of the *n*HH series as a function of alkoxy chain length. The S_A and S^*_C phases are present over the whole series from $n = 7$ to 12. The temperature range of existence of the former decreases with chain length, but that of the latter increases.

The $S^*_{C_\gamma}$ phase is observed with short chains (from $n = 7$ to 10) and disappears from $n = 11$. Its stability range is quite small (about 3°C), but wider than that of MHPOBC compound.

From $n = 8$ to $n = 12$, the ferri- and antiferro-electric phases are obtained.

3.2.4. *Racemic compounds*

Table 2 gives the transition temperature detected optically for the racemic derivatives ($n = 9$ to 12). Those compounds obviously show an odd-even effect with respect to the existence of the S_{CA} phase.

As suggested by previous results with the thiobenzoate series [5], the low temperature S_C phase of the dodecyl racemate could be a re-entrant phase. The binary diagram (see figure 4) with the undecyloxy homologue clearly demonstrates this character: this exhibits a large S_C domain surrounding the area of S_{C_A} phase, which disappears at a weight fraction of 70 wt % of dodecyloxy

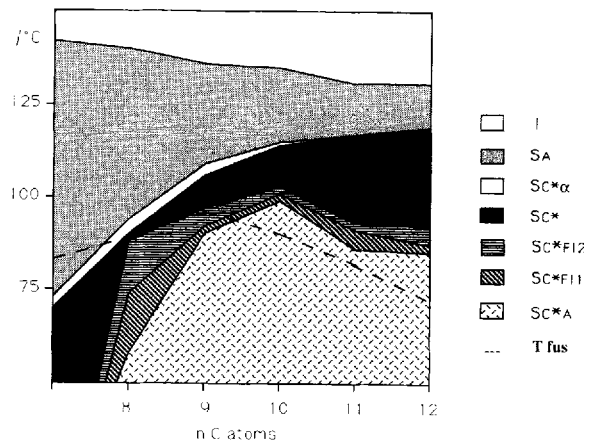

Figure 3 Phase behaviour of the *n*HH series as a function of alkoxy chain length.

Table 2. Transition temperatures (°C) for the racemic *n*HH compounds.

n	Cr		S_C		S_{C_A}		S_C		S_A		I
9	•	91·7	—		—		•	108	•	137·9	•
10	•	72	—		•	84	•	113·1	•	135	•
11	•	66	—		—		•	116	•	133·9	•
12	•	79·4	•	(56)	•	89·8	•	117·5	•	130·3	•

Parentheses denote a monotropic transition.

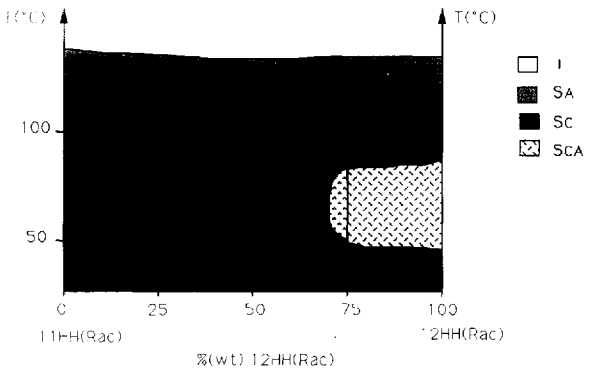

Figure 4. Isobaric phase diagram for the 11 and 12HH racemates.

compound, but it is difficult to determine the boundary with accuracy.

Then we can use this method to check the miscibility between the chiral nonyloxy enantiomer 9HH(R) and its homologous racemate (see figure 5). The binary diagram shows total miscibility between the two S_A phases, S_C^* and S_C, and $S_{C_A}^*$ and S_{C_A}. The transition $S_{C_A}^*$–$S_{C_{re}}^*$ progressively disappears (at $x = 50$ per cent). On the chiral side $S_{C_{FI}}^*$ quickly disappears (at $x = 20$ per cent). Note the optical purity required for this phase is higher than that for the thiobenzoate compounds. The $S_{C_\alpha}^*$ domain is much wider and persists up to 50 per cent.

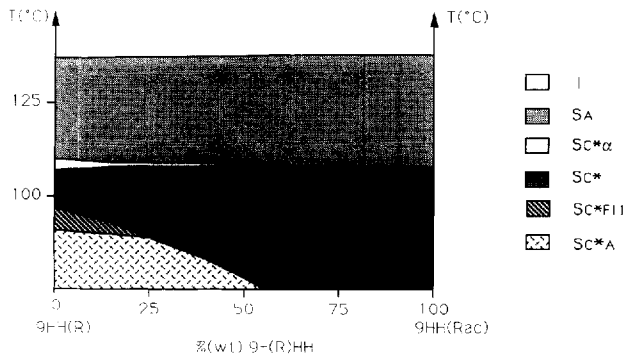

Figure 5. Isobaric phase diagram for 9(R)HH and its homologus racemate.

3.3. *Fluorinated compounds*

Tables 3, 4 and 5 give the temperatures and the enthalpies of the transitions, and figures 6, 7 and 8 show the phase behaviours as a function of the alkoxy chain length for the FH, HF, and FF series respectively.

For each series of compounds, the clearing temperature decreases with the chain length, whilst the ranges of temperature of the smectic A and $S_{C_\alpha}^*$ phases decrease, and those of the smectic S_C^* increase.

Comparing the four series, we note that the clearing temperatures (T_{Cl}) decrease in the order $T_{Cl}HH > T_{Cl}FF > T_{Cl}FH > T_{Cl}HF$. This order is in agreement with the results for the fluoro-substituted tolanes exhibiting the TGB_A phase [7].

No great difference between the series HH, FF, FH could be observed. They display the same rich polymorphism and their phase temperature ranges are comparable.

A more careful comparison shows a favouring of the $S_{C_\alpha}^*$ phase in the FF series (it persists until $n = 11$, as against $n = 10$ for the HH and the FH series).

The appearance of a second $S_{C_{FI}}^*$ phase when it exists seems to be linked to the chain length. Indeed, the FF series display both ferrielectric phases only with the shorter chains (up to $n = 11$).

The most striking result concerns the HF series. There, smectic A and $S_{C_\alpha}^*$ phases are considerably enhanced. It is very interesting to notice that for $n = 10$, the $S_{C_\alpha}^*$ phase has a wide enantiotropic temperature range of more than 8°C. Further physical studies of this phase are now in progress. In this series, ferri- and antiferro-electric phases disappear except for the long ones. All these phenomena are probably due to the coupling between the fluorine in the *meta*-position, with respect to the alkoxy chain, with the ester function.

4. Electro-optic properties

4.1. *Experimental procedure*

Electric field-dependent properties of the four decyloxy (10HH, 10FH, 10FF, 10HF) compounds have been investigated using commercial cells (from Linkam), coated with ITO (indium–tin oxide) over a 0·25 cm^2 active area. The thickness of the cells was 7·5 μm (obtained with two fibre glass spacers).

The inner surfaces are covered with unidirectionally rubbed polyamide layer, and slow cooling through the isotropic to S_A phase (0·1°C min^{-1}) transition leads to a planar alignment.

A classical electro-optical set-up was used for the measurements of switching current, response time and apparent tilt angle [8].

First, we note that transition temperatures for the materials in the cells are slightly different from those obtained for the bulk in thick samples, especially those for the ferro- to ferri- and ferri- to antiferro-electric transi-

Table 3. Transition temperatures (°C) and enthalpies (kJ mol^{-1}) (in italics) for the *n*FH series (positive enthalpy values are given for heating scans; negative ones are for cooling scans).

n	Cr		$S^*_{C_A}$		S^*_{CFI1}		S^*_{CFI2}		S^*_C		$S^*_{C_\alpha}$		S_A		I
8	•	87·4	•	91·5	•	97·0	—		—		•	100·4	•	132·5	•
		37·4		*− 0·008*		*− 0·01*		*− 0·10*				*− 0·037†*		*− 5·37*	
9	•	97·6	•	(95·8)	•	98·9	—		•	108·5	•	109·7	•	128·4	•
		43·7		*− 0·008*		*− 0·018*						*− 0·222†*		*− 5·38*	
10	•	89·3	•	101·8	•	103·4	—		•	112·8	•	113·3	•	127·1	•
		37·8		*− 0·013*		*− 0·029*						*− 0·243†*		*− 5·04*	
11	•	82·0	•	85·2	•	89·8	—		•	114·3	—		•	124·6	•
		36·9		*− 0·003*		*− 0·012*				*− 0·374*				*− 4·86*	
12	•	80·6	•	93·2	•	94·9	—		•	115·5	—		•	123·0	•
		37·7				*− 0·043†*				*− 0·480*				*− 4·62*	

† Sum of transition enthalpies.
Parentheses denote a monotropic transition.

Table 4. Transition temperatures (°C) and enthalpies (kJ mol^{-1}) (in italics) for the *n*HF series (positive enthalpy values are given for heating scans; negative ones are for cooling scans).

n	Cr		$S^*_{C_A}$		S^*_{CFI1}		S^*_{CFI2}	S^*_C		$S^*_{C_\alpha}$		S_A		I
8	•	57·6	—		—		—	—		—		•	126·4	•
		24·03											*− 5·53*	
9	•	75·5	—		—		—	•	(53·9)	•	(65·3)	•	123·1	•
		26·6							*− 0·002*		*− 0·004*		*− 5·34*	
10	•	75·6	—				—	•	(73·6)	•	84·1	•	122·6	•
		23·3							*− 0·002*		*− 0·007*		*− 5·49*	
11	•	75·2	—		—		—	•	92·5	•	95·8	•	120·3	•
		29·9							*− 0·008*		*− 0·030*		*− 5·42*	
12	•	66·3	•	(43·7)	•	73·3	—	•	98·9	•	100·8	•	118·9	•
		41·6							*− 0·006*		*− 0·027*		*− 5·48*	

Parentheses denote a monotropic transition.

Table 5. Transition temperatures (°C) and enthalpies (kJ mol^{-1}) (in italics) for the *n*HF series (positive enthalpy values are given for heating scans; negative ones are for cooling scans).

n	Cr		$S^*_{C_A}$		S^*_{CFI1}		S^*_{CFI2}		S^*_C		$S^*_{C_\alpha}$		S_A		I
8	•	72·2	—		—		—		—		•	(59·2)	•	135·7	•
		26·7										*− 0·006*		*− 5·33*	
9	•	71·1	•	76·8	•	79·2	•	84·7	•	89·3	•	94·5	•	131·8	•
		28·1		*− 0·001*		*− 0·001*		*− 0·006*		*− 0·007*		*− 0·026*		*− 5·13*	
10	•	56·1	•	91·2	•	92·7	•	95·0	•	100·8	•	103·5	•	130·3	•
		24·6		*− 0·011*		*− 0·003*		*− 0·010*		*− 0·011*		*− 0·004*		*− 5·18*	
11	•	58·8	•	70·5	•	71·4	•	80·5	•	108·6	•	109·5	•	127·7	•
		25·6						*− 0·008*				*− 0·174†*		− 5·02	
12	•	62·8	•	89·6	•	92·5	—		•	112·0	•	112.4	•	126·2	•
		36·0				*− 0·015†*						*− 0·264†*		*− 4·69*	

† Sum of transition enthalpies.
Parentheses indicate a monotropic transition.

tions. The hysteresis between cooling and heating is also greater than in the bulk. This behaviour is typical of these phases, and is probably due to the strong anchoring effect to the surfaces in a thin cell [9].

In order to avoid such problems, we chose to work with the same experimental conditions: all the experiments were carried out using increasing temperature with cells of the same thickness.

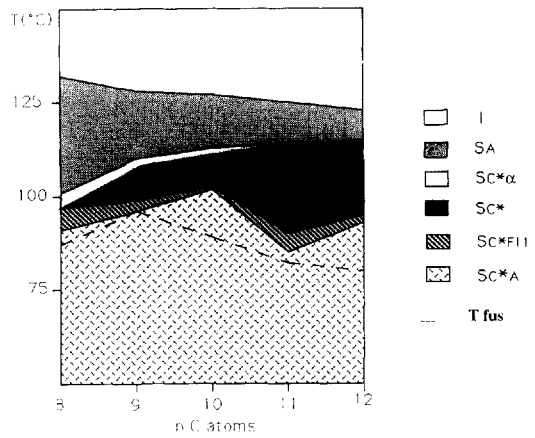

Figure 6 Phase behaviour of the *n*FH series as a function of alkoxy chain length

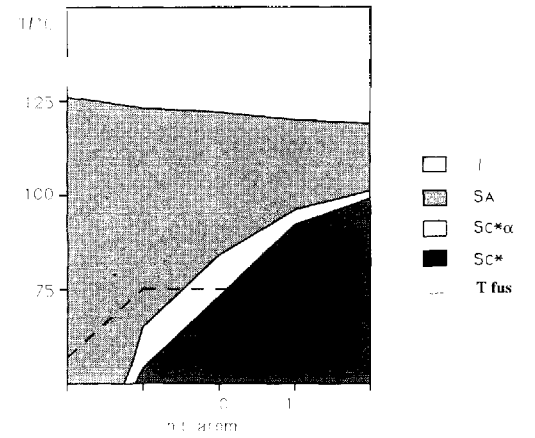

Figure 7. Phase behaviour of the *n*HF series as a function of alkoxy chain length

4.2. *Temperature dependence*

4.2.1. *Spontaneous polarization*

Those measurements were performed under an a.c. field at saturation ($E = \pm 4\,V\,\mu m^{-1}$; $\upsilon = 100\,Hz$). In these conditions, we studied the direct FO + /FO- transitions at various temperatures.

Figure 9 shows the behaviour under an a.c. field for the four chosen compounds. This behaviour is affected by the presence of the fluorine in the first phenyl ring. When the fluorine is in the *ortho*-position to the alkoxy chain, it raises the polarization values in the $S^*_{C_A}$ phase (100 instead of 80 nC cm^{-2}), whereas in the *meta*-position it lowers the polarization in the S^*_C phase (60 nC cm^{-2}). The difluoro-substituted compound behaves in an intermediate way. The polarization is little increased with respect to the hydrogenous material.

4.2.2. *Response time*

This is the time required for the majority of the molecules to switch under an a.c. field. It corresponds to the top of the polarization peak and is also affected by these substitutions (see figure 10). The fluorinated derivatives have higher response times than the hydrogenous material ones. Since the polarization of 10HH is lower than 10FH and 10FF, the increase in the response time could be explained by a viscosity effect due to the presence of the fluorine. Combining this viscosity effect and a low polarization value, the HF compound shows the slowest behaviour (more than 35 μs).

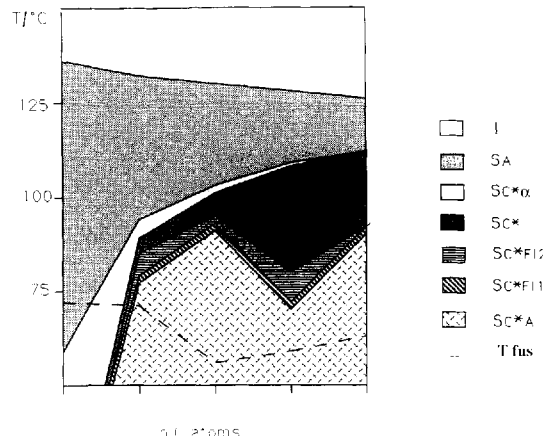

Figure 8 Phase behaviour of the *n*FF series as a function of alkoxy chain length

4.2.3. *Apparent tilt angle*

The angle from the normal to the layers in the smectic phases is measured in a classical way at very low frequency (0·1 Hz). The tilt angle values (see figure 11) seem to differ with the fluorine substitution in much the same order. Only the *n*HH and *n*FF series became inverted. They globally display the same electro-optic characteristics.

It is interesting to notice that the *n*FH series shows a breaking of the slope at the appearance of ferroelectric

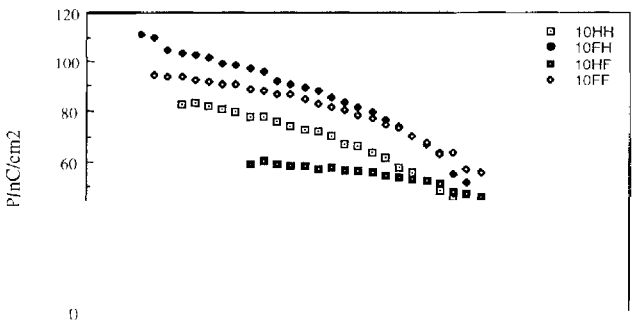

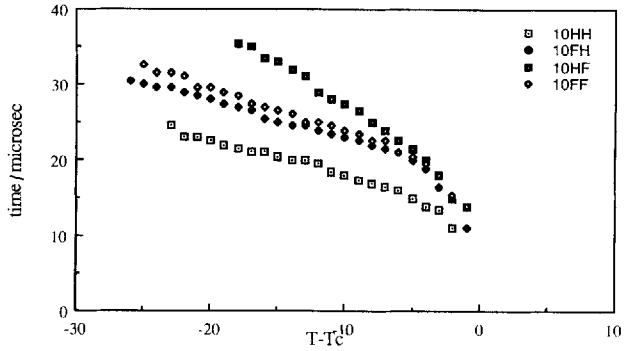

Figure 10. Response time versus temperature at saturation field ($E = \pm 4\,V\,\mu m^{-1}$ series; $\upsilon = 100\,Hz$); $T_c = T_{S_A}-S^*_{C_x}$.

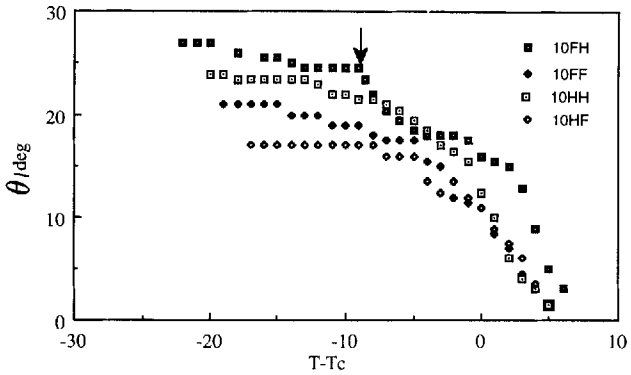

Figure 11. Apparent tilt angle versus temperature at saturation field ($E = \pm 4\,V\,\mu m^{-1}$; $\upsilon = 0{\cdot}1\,Hz$); $T_c = T_{S_A}-S^*_{C_x}$.

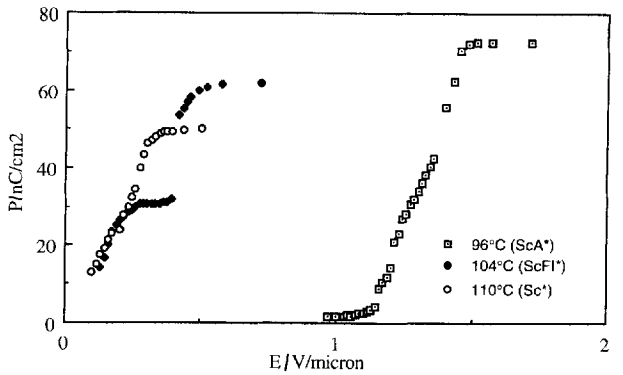

Figure 12. Polarization versus field for the *n*HH series at 96°C, 104°C and 110°C.

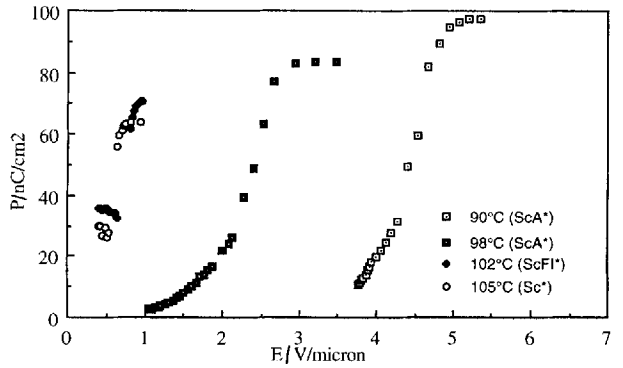

Figure 13. Polarization versus field for the *n*FH series at 90°C, 98°C, 102°C and 105°C.

anchoring (103·5°C) as the temperature increases. This phenomenon is not observed for the other series, but the change of slope may be too small to detect (due to the lower tilt values).

The difference between the 3-fluoro (FH) and 2-fluoro (HF) derivatives was previously observed by Booth *et al.* [10], with the chiral 1-methylheptyl 4′-[(2- or 3-fluorotetradecyloxyphenyl)propioloyloxy]biphenyl-4-carboxylates. The low value of the polarization ($60\,nC\,cm^{-2}$) of the HF material is tied to the low tilt angle (18°) by comparison with the FH material ($110\,nC\,cm^{-2}$ and 27°).

4.3. *Polarization versus a.c. field*

These measurements show significant differences from one phase to another. Figures 12, 13, 14, 15 represent the polarization dependence on the a.c. field in the S^*_C, $S^*_{C_{FI}}$ and $S^*_{C_A}$ phases.

The $S^*_{C_A}$ phase requires a relatively high field to accomplish transition to the ferroelectric phase. This threshold field decreases while the temperature increases (see figure 13).

In the $S^*_{C_{FI}}$ phases, the behaviour is similar, but at low field the polarization reaches a step at approximately *P*/2. This was previously observed for other types of materials in the $S^*_{C_{FI}}$ phases [5].

In the S^*_C phase, the saturation is easily reached with a field below $1\,V\,\mu m^{-1}$.

5. Discussion

The object of our study was to investigate the influence of fluorine substitution of the first phenyl ring of the benzoate esters, i.e. the variation of the transverse dipolar moment. Indeed, the Van der Waals radius of fluorine (1·35 Å) is not much higher than that of the hydrogen (1·1 Å). Thus the effect of steric hindrance on the existence of mesophases is less important, but is significantly observed on the clearing point.

Due to the three carboxy linkages, the hydrogenous materials possess a strong longitudinal moment, which is considerably increased by the presence of fluorine atom in the *meta*-position. The HF series seems to reach too high a value of this moment, which leads to a large stabilization of the S_A and $S^*_{C_x}$ phase, and the quasi disappearance of the $S^*_{C_A}$ and $S^*_{C_{FI}}$ phases. It has also an effect on the electro-optic behaviour.

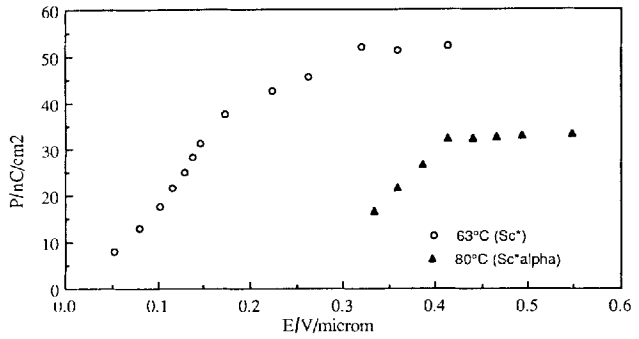

Figure 14. Polarization versus field for the *n*HF series at 63°C and 80°C.

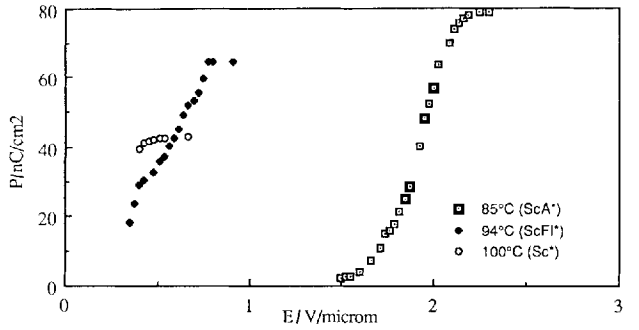

Figure 15. Polarization versus field for the *n*FF series at 85°C, 94°C and 100°C.

Fluorine in the *ortho*-position decreases the longitudinal moment and the whole mesophase sequence exists.

Difluoro-substitution increases this moment globally up to a medium value, which preserves the same mesophase sequence.

A comparison of the range of existence of the S_A phase of the four series clearly evidences the role of the dipole moment: for example, the S_A temperature range of the octyloxy derivatives of the FH, HH, FF and HF series are, respectively, 32·1, 45, 63·5 and 68·8°C (see table 6). A parallel comparison can be performed on the existence of the $S^*_{C_\gamma}$ phase: the chain length corresponding to its disappearance increases with the value of the longitudinal moment (10 for FH, 11 for HH, 12 for FF, and higher for HF). Due to this increase with the longitudinal moment, the S^*_C and $S^*_{C_A}$ phases are consequently less favoured. Therefore we can classify the influence of the fluoro substituents on the existence of S^*_C, $S^*_{C_{FI}}$, $S^*_{C_A}$ as: $HF \ll FF < HH < FH$.

Table 6. Temperature range (°C) of the S_A phase in the four series *n*HH, *n*FH, *n*HF and *n*FF, versus *n*.

	ΔT_{S_A}			
n	*n*HH	*n*FH	*n*HF	*n*FF
8	45	32·1	68·8	63·5
9	26·8	18·7	57·8	37·3
10	20·2	13·8	38·5	27·2
11	14	10·3	24·5	18·2
12	12·3	7·5	18·1	13·8

The various experiments clearly demonstrate that the materials (except the HF series) possess ferri- and antiferro-electric phases.

These series are built up with a benzoate core near the alkoxy chain, and it is of great interest to compare them with well-known compounds having a different chemical structure.

The first one reported in the literature was (*R*)- or (*S*)-4-(1-methylheptyloxycarbonyl)phenyl 4′-octyloxybiphenyl-4-carboxylate (MHPOBC) [1]. Since this discovery, other compounds have been synthesized possessing an alkoxy, alkanoyloxy of alkyl chain, with a different nature of the core:

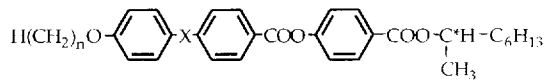

The group containing the linking group *X* was replaced by a thiobenzoate core [5] and more recently by a tolane core [11]. The compounds all display the same polymorphism, but the dependence upon the alkoxy chain length is different. When *n* is short ($n \leqslant 8$), the thiobenzoate and benzoate derivatives do not exhibit the entire polymorphism, whereas the tolane and biphenyl systems do. Moreover, the disappearance of $S^*_{C_\gamma}$ corresponds to $n \geqslant 10$ for the tolane series, $n \geqslant 11$ for the benzoate series, and $n \geqslant 16$ for the thiobenzoate series.

These facts can be explained by a variation of the local dipole moment of the central linking group *X*. Its increase by replacing tolane by a thiobenzoate or benzoate core delays the appearance of the various S^*_C phases. Table 7 summarizes the domain of the S_A phase depending on the nature of the linking group.

The transverse moment next to the chiral centre also influences the polymorphism. Up to now, polar smectic C* phases are found in materials possessing an ester linkage between the last phenyl ring and the chiral part. This

Table 7. Temperature range (°C) of the S_A phase with different core types (octyloxy derivatives).

X	—	C=C	COO	COS
ΔT_{S_A} ($n = 8$)	24	29·8	45	76·2

moment can be increased by a lateral substituent (Z) in compounds having the general formula:

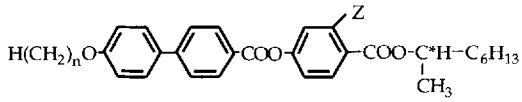

Demus *et al.* [12] reported their results with $Z = F$, where the materials display a wider $S^*_{C_A}$ temperature range. Other studies show the great importance of the longitudinal polarization, based on the conjugation between the chiral part and the core structure, on the appearance of antiferroelectricity [13]. The presence of methylene spacers between these two parts narrows the $S^*_{C_A}$ domain. This phase is also stabilized by introducing polar substituents such as CF_3 or C_2F_5 into the chiral centre.

Let us point out that the existence of these new polar smectic C* phases also depends on the nature of linking group Y in the following formula:

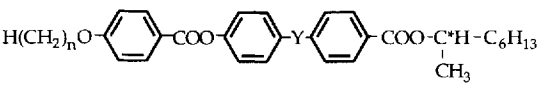

If Y is a non-polar symmetrical group such as that in a tolane [7] or an azobenzene core [14], these phases are not observed, and in most cases the formation of the TGB_A phase is favoured. If Y is a single bond, the biphenyl system represents a particular case, because the phenyl rings are not coplanar, which introduces a transverse moment. This behaviour favours the formation of different S^*_C phases [6]. The Y linking group therefore plays a very important role with regard to the existence of these phases.

Up to now, most antiferroelectric low molar mass compounds have been constituted of three phenyl rings or cyclic systems. Actually, however, shorter molecules exhibiting these phases do exist—for example the compound of structure:

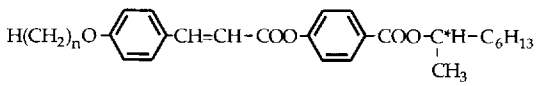

for $n = 7$ to 10 [15], but higher homologues ($n = 16, 18$) display a TGB_A phase [16].

6. Conclusions

The synthesis and characterization of these four different series with the formula:

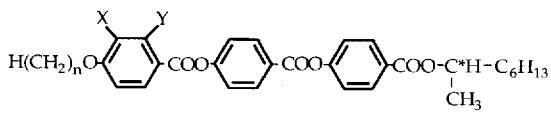

have allowed us to obtain several compounds exhibiting a very rich polymorphism with $S^*_{C_A}$, $S^*_{C_{FI}}$, S^*_C, $S^*_{C_\gamma}$ and S_A phases. They also indicate the effect of molecular parameters like steric hindrance and dipole moment on the existence of such phases. The comparison between these four series and those previously reported and having similar structures:

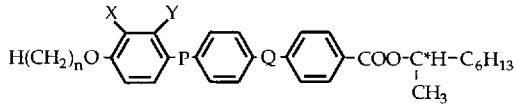

shows that:

(i) $S^*_{C_{FI}}$ and $S^*_{C_A}$ phases are favoured when Q has a transverse dipole moment, for example COO, COS. On the other hand, if Q is a symmetrical group (C ≡ C, N=N, ...) the TGB (Twist Grain Boundary smectic) is often observed.

(ii) Related to this first remark (Q=COO), the $S^*_{C_{FI}}$ and $S^*_{C_A}$ phases are less favoured with a polar P group, unlike the $S^*_{C_\alpha}$ phase. For example, the HF series (P=Q=COO, X=H, Y=F) does not display $S^*_{C_{FI}}$ and $S^*_{C_A}$ phases, but does exhibit a very large domain of $S^*_{C_\alpha}$ and S_A phases. This series is interesting for studies of $S^*_{C_\gamma}$, and not for other polar smectic C* phases.

(iii) The dipole moment of the COO group between the phenyl ring and the chiral chain is important for the appearance of these phases. If we replace this COO group by O, we only observe S_A and S^*_C phases [14].

(iv) The last remark concerns the FF series. As a consequence of its low fusion point, it exhibits a wide mesomorphic range, and a very rich polymorphism. Moreover, its polarization and its response time under an a.c. field are comparable to those of the HH series.

7. Experimental

7.1. *Synthesis of (R)-1-methylheptyl 4-benzyloxybenzoate* (3)

To a solution of (*R*)-octan-2-ol (13 g, 0·1 mol) in CH_2Cl_2 was added DCC (22·66 g, 0·11 mol), DMAP (1 g) and 4-benzyloxybenzoic acid (25·08 g, 0·11 mol). The mixture was stirred at room temperature overnight, filtered, the solvent evaporated and the residue purified by chromatography on silica gel using toluene as eluent. The resulting oil was used without further purification. Yield: 24·4 g, 71 per cent. ^{1}H NMR ($CDCl_3$): δ (ppm) = 0·88 (t, 3 H, CH_3 of C_6H_{13}), 1·3 (t, 6 H, $3CH_2$), 1·36 (d, 3 H, CH_3–CH), 1·6–1·8 (m, 2 H, CH_2–CHO), 5 (s, 2 H, CH_2O), 5·1 (m, 1 H, CH–CH_3), 6·9 (d, 2 H arom.), 7·3 (m, 5 H arom. of Ph–CH_2), 8 (d, 2 H, arom.). IR: 2931, 2859, 1709, 1606, 1510, 1251, 847, 771, 696 cm^{-1}.

7.2. *Synthesis of (R)-1-methylheptyl 4-hydroxybenzoate* (4)

(*R*)-1-methylheptyl 4-benzyloxybenzoate (24·4 g, 71 mmol) was dissolved in ethyl acetate (240 ml) and ethanol 95 per cent (60 ml), and 1·2 g of 10 per cent Pd/C was

added. Then hydrogen was added under a slight pressure. Hydrogen consumption stopped after about 4 h, after which the catalyst was filtered off and the solvent evaporated. The resulting oil was used without purification. Yield: 15·9 g, 89 per cent. ^{1}H NMR ($CDCl_3$): δ (ppm) = 0·88 (t, 3 H, CH_3 of C_6H_{13}), 1·3 (t, 6 H, $3CH_2$), 1·36 (d, 3 H, CH_3–CH), 1·6–1·8 (m, 2 H, CH, CH_2–CHO), 5·1 (m, 1 H, CH–CH_3), 6·9 (d, 2 H arom.), 7·9 (d, 2 H arom.). IR: 3346, 2931, 2859, 1710, 1606, 1514, 1251, 851, 773, 699 cm^{-1}.

7.3. *Synthesis of (R)-1-methylheptyl 4-(4-benzyloxybenzoyloxy)benzoate* (**5**)

To a solution of (*R*)-1-methylheptyl 4-hydroxybenzoate (15·9 g; 63 mmol) in CH_2Cl_2 was added DCC (14·4 g, 69 mmol), DMAP (0·7 g) and 4-benzyloxybenzoic acid (15·95 g, 69 mmol). The mixture was stirred at room temperature overnight, filtered, the solvent evaporated and the residue purified by chromatography on silica gel using toluene as eluent. In addition, the product was recrystallized from absolute ethanol, yielding 24·17 g, 82 per cent, m.p. 99°C. ^{1}H NMR ($CDCl_3$): δ (ppm) = 0·88 (t, 3 H, CH_3 of C_6H_{13}), 1·25 (t, 6 H, $3CH_2$), 1·36 (d, 3 H, CH_3–CH), 1·6–1·8 (m, 2 H, CH_2–CHO), 4·85 (m, 1 H, CH–CH_3), 4·9 (s, 2 H, CH_2O), 7·04 (d, 2 H arom.), 7·26 (d, 2 H arom.), 7·4 (m, 5 H arom. of Ph–CH_2), 8·1 (d, 2 H, arom.). IR: 2931, 2859, 1710, 1606, 1510, 1251, 851, 773, 699 cm^{-1}.

7.4. *Synthesis of (R)-1-methylheptyl 4-(4-hydroxybenzoyloxy)benzoate* (**6**)

(*R*)-1-methylheptyl 4-(4-benzyloxybenzoyloxy)benzoate (24·1 g, 52 mmol) was dissolved in ethyl acetate (240 ml) and ethanol 95 per cent (60 ml), and 1·2 g of 10 per cent Pd/C was added. Then hydrogen was added under a slight pressure. Hydrogen consumption stopped after about 3 h, after which the catalyst was filtered off and the solvent evaporated. The solid residue was recrystallized from heptane–ethyl acetate (1 : 9) mixture. Yield: 15·56 g, 79 per cent, m.p. 80°C. ^{1}H NMR ($CDCl_3$): δ (ppm) = 0·88 (t, 3 H, CH_3 of C_6H_{13}, 1·25 (t, 6 H, $3CH_2$), 1·36 (d, 3 H, CH_3–CH), 1·6–1·8 (m, 2 H, CH_2 CHO), 5·2 (m, 1 H, CH–CH_3), 7·0 (d, 2 H arom.), 7·5 (d, 2 H arom.), 8·2 (d, 2 H arom.), 8·4 (d, 2 H arom.). IR: 3405, 2931, 2859, 1698, 1590, 1512, 1273, 845, 762, 691 cm^{-1}.

7.5. *Synthesis of (R)-4-(1-methylheptyloxycarbonyl)phenyl 4'-(4-decyloxybenzoyloxy)benzoate*

To a solution of (*R*)-1-methylheptyl 4-(4-hydroxybenzoyloxy)benzoate (0·3 g, 0·8 mmol) in CH_2Cl_2 was added DCC (0·18 g, 0·88 mmol), DMAP (9 mg) and 4-decyloxybenzoic acid (**7**) (0·24 g; 0·88 mmol). The mixture was stirred at room temperature overnight, filtered, the solvent evaporated and the residue purified by chromatography on silica gel using CH_2Cl_2 as eluent. In addition, the product was recrystallized from absolute ethanol, yielding 0·31 g, 63 per cent. ^{1}H NMR ($CDCl_3$): δ (ppm) = 0·88 (t, 6 H, $2CH_3$), 1·25 (m, 22 H, $11CH_2$), 1·36 (d, 3 H, CH_3–CH), 1·6–1·8 (m, 4 H, $2CH_2$), 4 (t, 2 H, OCH_2), 5·2 (m, 1 H, CH–CH_3), 7·23 (m, 4 H, arom.), 7·36 (d, 2 H arom.), 8·1 (d, 2 H arom.), 8·26 (m, 4 H arom.). IR: 2923, 2853, 1738, 1686, 1513, 1271, 846, 765, 691 cm^{-1}.

The authors would like to express their gratitude to J. F. Guérit for miscibility studies with the racemic compounds, A. Babeau for synthesizing the fluorinated benzoic acids, and P. Cluzeau for his help during the electro-optic measurements.

References

[1] Chandani, A. D. L., Ouchi, Y., Takezoe, H., Fukuda, A., Furukawa, K., and Kichi, A., 1989, *Jap. J. appl. Phys.*, **28,** 1261.
[2] Fukuda, A., Takanishi, Y., Isozaki, T., Ishikawa, K., Takezoe, H., 1994, *J. mater. Chem.*, **4,** 997.
[3] Nabor, M. F., Nguyen, H. T., Destrade, C., Marcerou, J. P., and Twieg, R. J., 1991, *Liq. Crystals*, **10,** 785.
[4] Kelly, S. M., 1989, *Helv. Chim. Acta*, **72,** 594.
[5] Nguyen, H. T., Rouillon, J. C., Cluzeau, P., Sigaud, G., Destrade, C., and Isaert, N., 1994, *Liq. Crystals*, **17,** 571.
[6] Goodby, J. W., Patel, J. S., and Chin, E., 1992, *J. mater. Chem.*, **2,** 197.
[7] Nguyen, H. T., Twieg, R. J., Nabor, M. F., Isaert, N., and Destrade, C., 1991, *Ferroelectrics*, **121,** 187.
[8] Dupont, L., Glogarova, M., Marcerou, J. P., Nguyen, H. T., and Destrade, C., 1991, *J. Phys. II*, **1,** 831.
[9] Moritake, H., Shigeno, N., Ozaki, M., and Yoshino, K., 1993, *Liq. Crystals*, **14,** 1283.
[10] Booth, C. J., Dunmur, D. A., Goodby, J. W., Kang, J. S., and Toyne, K. J., 1994, *J. mater. Chem.*, **4,** 747.
[11] Cluzeau, P., Nguyen, H. T., Destrade, C., Isaert, N., Barois, P., and Babeau, A., 1994, *15th International Liquid Crystal Conference*, Budapest, A-Inv 1.
[12] Demus, D., Inuka, T., Saito, S., and Goto, Y., 1994, *15th International Liquid Crystal Conference*, Budapest, Plen4.
[13] Suzuki, Y., Nonaka, O., Koide, Y., Okabe, N., Hagiwara, T., Kawamura, I., Yamamoto, N., Yamada, Y., and Kitazume, T., 1993, *Ferroelectrics*, **147,** 109.
[14] Unpublished results.
[15] Heppke, G., Hollidt, J. M., Moro, D., Lötzsch, D., Tuffin, R. P., and Goodby, J. W., 1994, *15th International Liquid Crystal Conference*, Budapest, J-Sbp9.
[16] Nguyen, H. T., Destrade, C., Parneix, J. P., Pochat, P., Isaert, N., and Girold, C., 1993, *Ferroelectrics*, **147,** 181.